

Mechanical and Thermal Properties of Glass Reinforced Composites

V. J. Toplosky, S. B. Betts , R. E. Goddard, J. A. Torres, D. N. Nguyen , and K. Han 

Abstract—In our Pulsed Field Facility, we use epoxy fillers to create smooth, strong winding transitions between layers of coils in our consumable pulsed magnets. For structural support, we often use materials like G10, a high-pressure fiberglass laminate consisting of multiple glass layer cloths soaked in epoxy. In liquid nitrogen, such materials have good mechanical and dielectric strength. To accommodate gaps at transitions, epoxy fillers typically have complex shapes, which render their fabrication expensive and time-consuming. In addition, the machining of epoxies like G10 can be hazardous. In this study, we replaced machining with 3D printing, using thermo-plastic, strengthened by glass fiber, as the raw material. Polyether Ether Ketone (PEEK) material as well as nylon material were used as the matrix. The strengthening components were chopped E-glass fibers or beads. We found that 3D printing can significantly reduce manufacturing cost for our magnets. Because our magnets must operate between 77 K and 295 K, we measured mechanical and thermal properties for both the nylon and the PEEK composites at both temperatures. The measured direction of the samples was parallel to the printing direction. The measured maximum compressive strength was about 258 MPa. Although the strength is lower than G10, the techniques we developed in this study would apply to 3D printing technology for various cryogenic applications like winding transition or experimental probes that are not exposed to very high stress in high field magnets.

Index Terms—Cryogenic, mechanical strength, polymers, pulsed magnets, thermal contraction.

I. INTRODUCTION

THE magnets used at the Pulsed Field Facility at the National High Magnetic Field Laboratory (NHMFL) have a finite lifetime. Coils are replaced as needed. The current design uses fillers made of G10 CRYogenic (G10 CR, a high-pressure fiberglass laminate) to act as spacers to guide the magnet conductor wires through the layers of winding and the transitions between them [1]–[2]. G10 performs well; it has excellent compressive

Manuscript received January 7, 2022; revised April 19, 2022, April 28, 2022, and June 1, 2022; accepted June 6, 2022. Date of publication June 10, 2022; date of current version June 21, 2022. The work was undertaken in the National High Magnetic Field Laboratory, which is supported by NSF DMR-1644779 and the State of Florida. The microscopes were funded by Florida State University Research Foundation and Florida State. (*Corresponding author: K. Han.*)

V. J. Toplosky, R. E. Goddard, and K. Han are with the National High Magnetic Field Laboratory, Florida State University, Tallahassee, FL 32310 USA (e-mail: toplosky@magnet.fsu.edu; han@magnet.fsu.edu).

S. B. Betts, J. A. Torres, and D. N. Nguyen are with the Pulsed Field Facility (NHMFL), Los Alamos National Laboratory, Los Alamos, NM 87545 USA (e-mail: doan@lanl.gov).

Color versions of one or more figures in this article are available at <https://doi.org/10.1109/TASC.2022.3181574>.

Digital Object Identifier 10.1109/TASC.2022.3181574

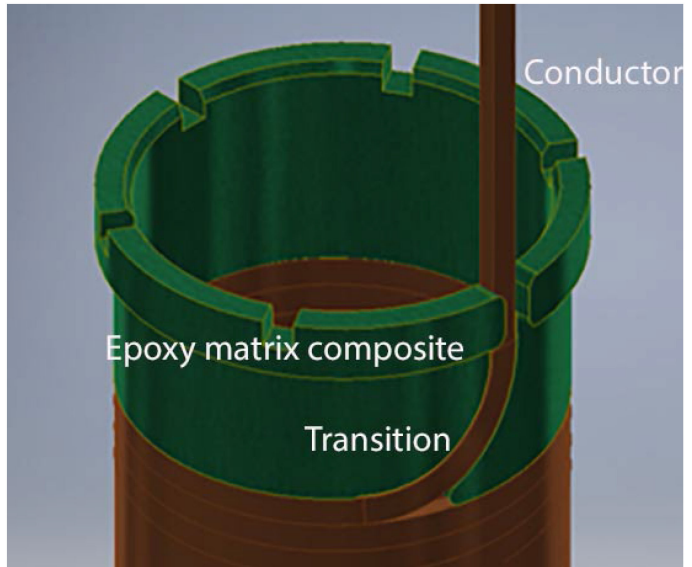


Fig. 1. Image showing a typical transition portion of the G10 filler/spacer and conductor turn. The locations of the G10 filler and conductor are complex (consisting of many different and connected parts.).

strength (>600 MPa at 77 K) and good thermal properties in the liquid nitrogen that is used to cool the magnet down during operation [3]. G10 CR, however, has long manufacturing lead times because it is difficult and hazardous to machine using conventional methods [4]–[5].

When fillers require complex geometry, as in transitions between winding layers, they must be machined before installation (Figs. 1 and 2). This machining is responsible for one of the major costs of pulsed magnet construction. To reduce costs, we explored the possibility of using 3D printing technology to manufacture fillers. We tested two thermoplastic candidates as raw materials: glass-filled PolyEther Ether Ketone (PEEK) and glass-filled nylon—both of which are suitable for 3-D printing.

Compressive strength is essential for pulsed magnet applications because fillers undergo large compressive loads during magnet operation. Hence, we performed mechanical tests (tensile and compression) on both materials. We also used dilatometry to measure the thermal expansion coefficient on both materials because low thermal expansion can lead to loose fits, and large thermal expansion can lead to cracking of the filler structure.

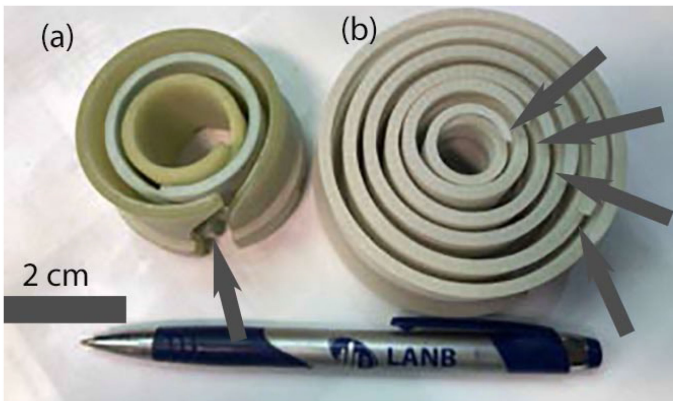


Fig. 2. Two examples of complex shaped fillers for pulsed magnets for National High Magnetic Field Laboratory. A pen and a centimeter bar in the image show the size of the fillers. The arrows point to the locations with complex shapes. (a) Fillers made of G10. (b) Fillers made of PEEK.

II. EXPERIMENTAL METHODS

A. Materials

We acquired both compressive (cylindrical) and tensile (rectangular) samples of glass-filled nylon (PA 3200 GF) and PEEK+GF20 composites, each reinforced with about 20% glass particles.

Using their Selective Laser Sintering (SLS) printer, 3D Systems Corp. produced PA 3200 samples based on nylon 12 (formula $[(\text{CH}_2)_{11}\text{CNH}]_{11}$) [6]. SLS is a powder-based 3D printing technology. It uses a laser to fuse material layers into a final part by tracing the pattern of each cross section of a 3D design onto a bed of powder. After one layer is built, the build platform is lowered, and another layer is built on top of the previous layer. This process continues until the part is complete. For the GF nylon samples, glass-fiber microbeads were blended into the base powder materials [7].

3DXtech Corp. made our PEEK+GF20 samples (formula $\text{C}_{19}\text{H}_{14}\text{F}_2\text{O}$) using a Fused Deposition Modeling (FDM) 3D printing system with glass microfibers mixed into a polymer filament wound around a spool. This material was “knitted,” layer by layer, into the shape of the part.

B. Mechanical Testing

Both the compressive and tensile tests were performed on a 100 kN MTS servo-hydraulic test system. Tests were performed at room temperature (295 K) and liquid nitrogen (77 K).

For the compressive tests, five samples were tested for each temperature condition. The 12.7 mm diameter by 25 mm long samples were compressed at a rate of 0.5 mm/sec until failure (Fig. 3(a)). Testing was performed as per ASTM standard D695 [8].

Tensile test samples were machined to a gage length of 25 mm and rectangular cross-section of $3 \times 6 \text{ mm}^2$ from $6.5 \times 13 \text{ mm}^2$ cross-section bar. The samples were loaded in displacement control mode at a rate of 0.5 mm/sec until failure. A 25 mm clip-on extensometer was used to record sample strain (Fig. 3(b)). Three samples were conducted for each temperature. Testing

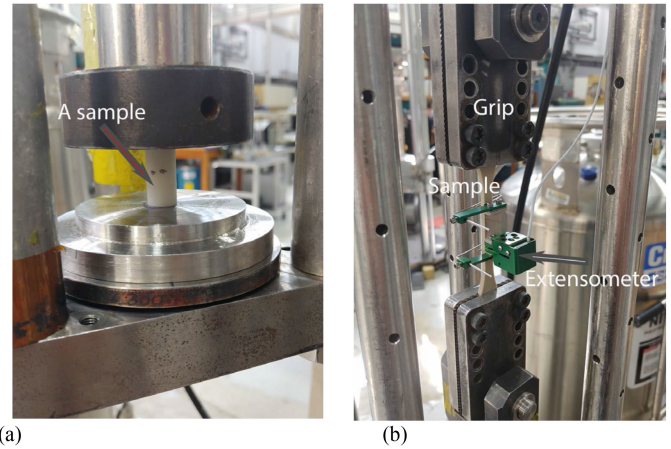


Fig. 3. Typical set up of mechanical testing of composites. The test rigs can be immersed in a liquid nitrogen dewar for testing at 77 K. (a) Compressive test rig. The white rod in the middle is a compressive test sample. (b) Tensile tests rig. The metal plates at the top and bottom of the image are grips that work at cryogenic temperatures.

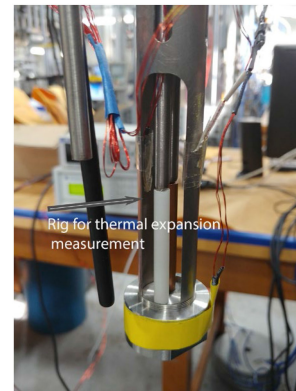


Fig. 4. Fixture of thermal contraction measurements. The fixture can be immersed in liquid nitrogen or helium.

was conducted as per ASTM standard D638 [9]. From the measured stress-strain curves, both ultimate tensile strength (TS) and 0.2% offset engineering flow stress ($\text{YS} = \text{Yield Strength}$) are calculated.

C. Thermal Testing

Thermal expansion measurements were performed on a dilatometer composed of a quartz tube specimen holder, a counterweighted quartz pushrod that makes light contact with the specimen and a fiber optic displacement sensor tracking movement of the pushrod. The specimen was submerged in liquid helium (4.2 K) and naturally warmed to room temperature (Fig. 4). Three samples were tested for each material and testing followed ASTM Standard D696 [10].

D. Microstructure Examination

Both the PEEK and nylon rods were sectioned laterally and hot-mounted (at about 423 K) in a Bakelite cylindrical puck with a 25 mm diameter. The samples were wet ground with 500 and

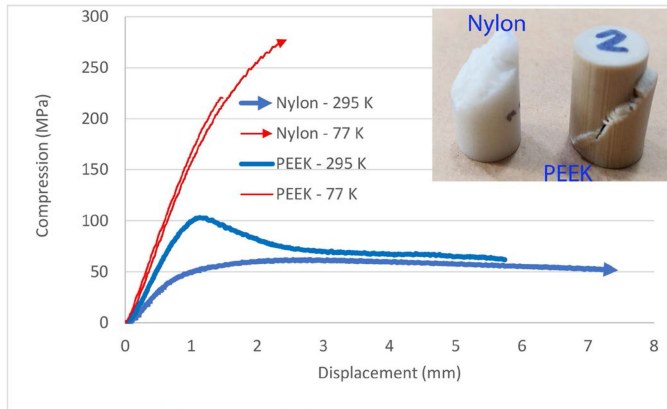


Fig. 5. Compressive stress vs. specimen displacement of the two composites. The thick and thin solid curves are from data collected at 295 and 77 K, respectively. The curves with and without arrows are from data for nylon and PEEK, respectively. An inset shows fractured compression samples tested at room temperature. The tested sample shows a typical 45-degree shear failure.

TABLE I
TENSILE TEST RESULTS-NYLON

Temp (K)	Modulus (GPa)	Yield Strength (MPa)	Tensile Strength (MPa)	Elong. (%) 25 mm GL
295	2.8	22	31	6.2
77	7.8	92	95	1.4

800 grit SiC paper. The samples were then polished with 9 and 3 μm polycrystalline diamond solutions. A final polish of 0.04 μm alumina particles in a slurry of approximately 9 pH was used on a vibrator polisher. Glass particles tended to break off and pull out yielding some additional scratches on the polished surface. The samples were then analyzed using a laser confocal microscope (Olympus LEXT OLS3000).

III. RESULTS

A. Uniaxial Mechanical Strength and Elongation

At room temperature and under compression, typical compressive strength/displacement curves showed that the PEEK matrix composites were stronger than the nylon matrix composites. The deformation behavior of PEEK appeared similar to data from other researchers [11]–[12]. Both materials exhibited softening at larger strain values, PEEK significantly more than nylon (Fig. 5). We observed shear failure in both composites, indicating large plastic deformation (Fig. 5 inset).

At 77 K, the strength values of nylon increased by 300%, surpassing those of PEEK, which increased much less. Samples from both composites showed embrittlement at failure.

At room temperature and under tension, typical stress-strain curves showed that PEEK was stronger than nylon (Fig. 6). At 77 K, even though nylon demonstrated a significant strength increase, the PEEK matrix composite still showed higher mechanical strength than nylon (Tables I and II). We believe that differences between the two composites tested at two different

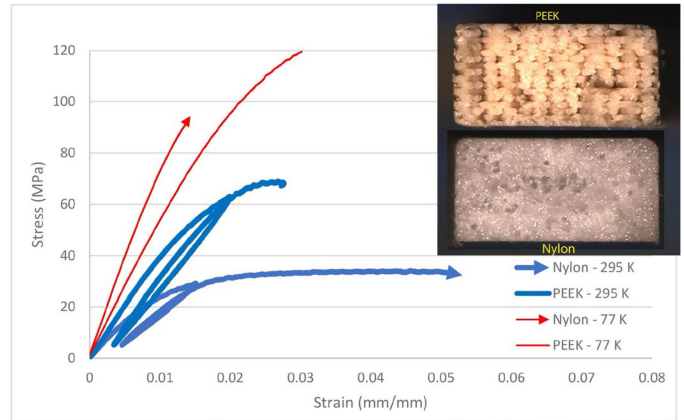


Fig. 6. Stress-strain curves of the two composites tested at 295 K (thin curves) and 77 K (thick curves). The curves with an arrow are from nylon. The curves without arrow are from PEEK. An inset shows the fractured surface of both composites.

TABLE II
TENSILE TEST RESULTS-PEEK

Temp (K)	Modulus (GPa)	Yield Strength (MPa)	Tensile Strength (MPa)	Elong. (%) 25 mm GL
295	4.2	52	68	3.0
77	5.5	92	114	2.7

TABLE III
LINEAR THERMAL EXPANSION COEFFICIENTS

Coeff.	a	b	c	d	e
Nylon	-1.351	4.116×10^{-4}	1.571×10^{-5}	-5.850×10^{-9}	3.883×10^{-12}
PEEK	-0.5047	2.770×10^{-4}	1.256×10^{-5}	-4.592×10^{-9}	6.789×10^{-12}

temperatures resulted from the rigidity of the molecular chain and the distribution of the strengthening component. Fractural surface images of nylon and PEEK showed flat and rigged features, respectively, indicating fiber strengthened composite had more fractured area than that strengthened by beads (inset in Fig. 6).

B. Thermal Contraction

When we measured thermal expansion for both composites, we found that the thermal contraction of nylon was almost three times of that of PEEK—a value of -1.2% for nylon compared to -0.43% for PEEK at 77 K (Fig. 7). The thermal expansion G10 CR has a thermal expansion between these two composites [13]. We found that the signs for two composites were the same for the coefficients in an equation $a+bT+cT^2+dT^3+eT^4$ to describe the thermal expansion (Table III).

C. Distribution of Glass Particles

Cross-sectional images showed that the volume fraction of reinforcement particles in both composites was close to 20 vol%,

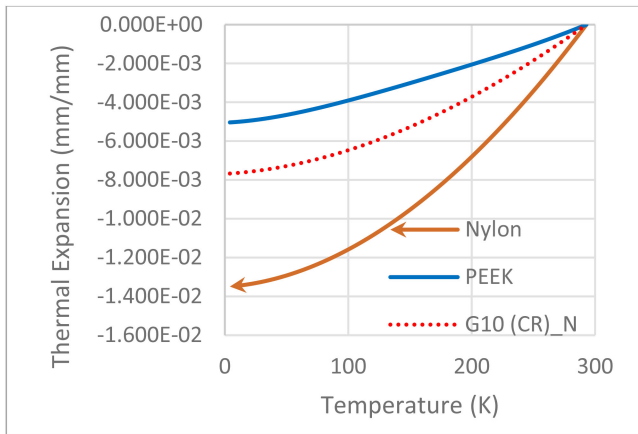


Fig. 7. Thermal expansion between 295 and 4.2 K. The curve with an arrow is from nylon and the one without arrow is from PEEK. The dashed line is from G10 from published results from others for comparison.

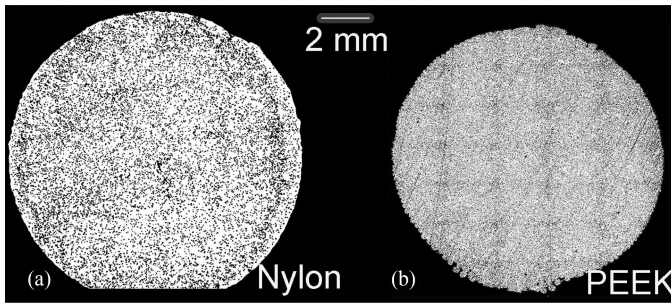


Fig. 8. Cross-section images of nylon (a) and PEEK (b) matrix composites. The measured volume fraction is 19.1% in nylon and 20.4% in PEEK. The measured median diameter of the circular cross section of the particles in the nylon matrix is 49 μm , which is greater than fibers measured for PEEK (20 μm).

with the value for PEEK marginally larger (Fig. 8). The volume fraction values were analyzed by binarizing and analyzing the images. These particles appeared to be more homogeneously distributed in PEEK than in nylon.

Larger magnification images revealed both the distribution and the particle diameters of glass particles. The average diameter of the particles in nylon was roughly twice that of the particles in PEEK. In both composites, all particles were smaller than 50 μm (Fig. 8).

IV. DISCUSSION

At room temperature, we observed softening of both composites in compression. We observed no softening during the tensile tests – the failure was noticeably brittle. In metals or metal-metal composites, softening is attributed to dynamic recovery [14]–[23]. The softening in current work is attributed to the buckling of the strengthening components accompanied by significant shearing of the composite during compression tests and not in tension. The buckling and shearing difference can be related to the diameter and shape of the strengthening components. PEEK was strengthened by short fiber with smaller diameter and finer spacing, whereas nylon was strengthened

by beads with larger diameter and coarse spacing. Buckling of strengthening component occurred mainly in PEEK. It appears that cryogenic temperature led to stiffer material properties, similar to what we observed in metallic structural materials for magnets [24]–[30]. Hence, no softening was observed in the 77 K tests.

Although cryogenic temperature led to higher mechanical strength, it reduced ductility in both composites. This change of the properties may be related to the reaction of polymer chains to reduced temperatures. At 77 K, the mobility of the polymer chains was reduced, and the polymer chains were more rigid [31]–[40]. Our experimental data on modulus indicated that the rigidity increase was higher for nylon than PEEK. Therefore, although at room temperature nylon composite samples had lower yield strength and compressive strength than those of PEEK, at 77 K they reached same yield strength as those of PEEK and even higher compressive strength than those of PEEK.

The property data indicated that the materials showed much higher ultimate mechanical strength at compression than tension. This indicates that for magnet applications, these composites should be avoided if exposed to too much tensile loading.

The strength values of 3D-printed composites were lower than those of G10 CR and significantly lower than Zylon strengthened composites [3], [41], [42]. The difference was attributed to the volume fraction and geometry of the strengthening components, and the voids formed during the 3D-printing. The voids, which impacted more on tensile strength than compressive strength, also caused that the tensile strength values of our 3D-printed materials weaker than those of bulk nylon (84 MPa) and PEEK (137 MPa). Although the glass particles were included for strengthening of the composites, the imperfection of the interface between the matrix and strengthening components led to generation of voids. Wetting between glass and matrix needs to be considered for making such composites in future work.

Most polymer-based composites show anisotropic properties [42]. This is particularly true for thermal expansion. We are planning experiments on characterize our composites in other orientations.

V. CONCLUSION

Both of our glass-particle-strengthened, 3D-printed samples—one of nylon and the other of PEEK—showed good compressive strength. Nylon, which was strengthened by larger diameter beads, showed higher compressive strength at 77 K and higher thermal expansion at cryogenic temperatures. PEEK, which was strengthened by chopped fibers, showed higher tensile strength at 77 K. We attributed these differences to differences in matrix stiffness and particle distributions.

ACKNOWLEDGMENT

The authors would like to thank Mr. R. Walsh and Mr. A. Atallah for their help in thermal expansion measurements and Dr. M. Tyler for editing.

REFERENCES

- [1] C. A. Swenson *et al.*, "Performance of 75 T prototype pulsed magnet," *IEEE Trans. Appl. Supercond.*, vol. 16, no. 2, pp. 1650–1655, Jun. 2006.
- [2] C. A. Swenson *et al.*, "Pulse magnet development program at NHMFL," *IEEE Trans. Appl. Supercond.*, vol. 14, no. 2, pp. 1233–1236, Jun. 2004.
- [3] R. P. Walsh, J. D. McColskey, and R. P. Reed, "Low-temperature properties of a unidirectionally reinforced epoxy fiberglass composite," *Cryogenics*, vol. 35, no. 11, pp. 723–725, Nov. 1995.
- [4] H. J. Schneider-Muntau, K. Han, N. A. Bednar, C. A. Swenson, and R. Walsh, "Materials for 100 T monocoil magnets," *IEEE Trans. Appl. Supercond.*, vol. 14, no. 2, pp. 1153–1156, Jun. 2004.
- [5] J. R. Sims, J. B. Schilling, C. A. Swenson, D. L. Gardner, A. N. Matlashov, and C. N. Ammerman, "Low-Noise pulsed pre-polarization magnet systems for ultra-low field NMR," *IEEE Trans. Appl. Supercond.*, vol. 20, no. 3, pp. 752–755, Jun. 2010.
- [6] D. Compare, "Pa 3200GF;" Nov. 19, 2021. [Online]. Available: <https://3dcompare.com/materials/products/pa-3200-gf>
- [7] PEEK. [Online]. Available: <https://www.boedeker.com/family/peek?msclkid=df02b443bc1711ecb7e900b4f5fe51d7>
- [8] *Standard Test Method for Compressive Properties of Rigid Plastics*, A. I. ASTM Standard D 695M, Philadelphia, PA, USA, D 256-D 2343, 1991, 1994.
- [9] *Standard Test Method for Tensile Properties of Plastics*, ASTM Standard D 683M, P. ASTM International, PA, Volume 08.01 Plastics (I), D 256-D 2343, 1994.
- [10] P. ASTM International, PA, "Standard test method for coefficient of linear thermal expansion of plastics between -30°C and 30°C ," 1991.
- [11] M. C. Boyce and E. M. Arruda, "An experimental and analytical investigation of the large strain compressive and tensile response of glassy polymers," *Polym. Eng. Sci.*, vol. 30, no. 20, pp. 1288–1298, Oct. 1990.
- [12] F. Chen, H. A. Ou, B. Lu, and H. Long, "A constitutive model of polyether-ether-ketone (PEEK)," *J. Mech. Behav. Biomed. Mater.*, vol. 53, pp. 427–433, Jan. 2016.
- [13] E. D. Marquardt, J. P. Le, and R. Radebaugh, "Cryogenic material properties database," pp. 681–687, 2001.
- [14] K. Han, R. P. Walsh, A. Ishmaku, V. Toplosky, L. Brandao, and J. D. Embury, "High strength and high electrical conductivity bulk Cu," *Philos. Mag.*, vol. 84, no. 34, pp. 3705–3716, Dec. 2004.
- [15] J. Chen, K. Han, P. N. Kahl, and W. D. Markiewicz, "Deformation behavior of Nb_3Sn type superconductors," *IEEE Trans. Appl. Supercond.*, vol. 15, no. 2, pp. 3568–3571, Jun. 2005.
- [16] C. A. Davy, K. Han, P. N. Kalu, and S. T. Bole, "Examinations of Cu-Ag composite conductors in sheet forms," *IEEE Trans. Appl. Supercond.*, vol. 18, no. 2, pp. 560–563, Jun. 2008.
- [17] K. Han, V. J. Toplosky, R. Goddard, J. Lu, R. Niu, and J. Chen, "Impacts of heat treatment on properties and microstructure of Cu16at% Ag conductors," *IEEE Trans. Appl. Supercond.*, vol. 22, no. 3, Jun. 2011, Art. no. 6900204.
- [18] R. M. Niu and K. Han, "Strain hardening and softening in nanotwinned Cu," *Scripta Materialia*, vol. 68, no. 12, pp. 960–963, Jun. 2013.
- [19] R. M. Niu, K. Han, Y. F. Su, T. Besara, T. M. Siegrist, and X. Zuo, "Influence of grain boundary characteristics on thermal stability in nanotwinned copper," *Sci. Rep.*, vol. 6, Aug. 2016, Art. no. 31410.
- [20] C. Zhao *et al.*, "Improvement of properties in Cu–Ag composites by doping induced microstructural refinement," *Mater. Sci. Eng.: A*, vol. 799, 2021, Art. no. 140091.
- [21] C. C. Zhao, X. W. Zuo, E. G. Wang, and K. Han, "Strength of Cu-28 wt%Ag composite solidified under high magnetic field followed by cold drawing," *Met. Mater. Int.*, vol. 23, no. 2, pp. 369–377, Mar. 2017.
- [22] C. C. Zhao, X. W. Zuo, E. G. Wang, R. Niu, and K. Han, "Simultaneously increasing strength and electrical conductivity in nanostructured Cu-Ag composite," *Mater. Sci. Eng. a-Struct. Mater. Properties Microstructure Process.*, vol. 652, pp. 296–304, Jan. 2016.
- [23] X. W. Zuo, R. Guo, C. C. Zhao, L. Zhang, E. Wang, and K. Han, "Microstructure and properties of Cu-6Wt% Ag composite thermomechanical-processed after directionally solidifying with magnetic field," *J. Alloys Compounds*, vol. 676, pp. 46–53, Aug. 2016.
- [24] K. Han *et al.*, "Mechanical properties of MP35N as a reinforcement material for pulsed magnets," *IEEE Trans. Appl. Supercond.*, vol. 12, no. 1, pp. 1244–1247, Mar. 2002.
- [25] K. Han, J. R. Sims, C. A. Swanson, and H. J. Schneider-Muntau, "Reinforcement materials for high field magnets," *IEEE Trans. Appl. Supercond.*, vol. 14, no. 2, pp. 1141–1144, Jun. 2004.
- [26] A. Ishmaku and K. Han, "Deformation induced nanostructure and texture in MP35N alloys," *J. Mater. Sci.*, vol. 39, no. 16-17, pp. 5417–5420, Aug./Sep. 2004.
- [27] V. J. Toplosky and K. Han, "Mechanical properties of cold-rolled and aged MP35N alloys for cryogenic magnet applications," in *Proc. Adv. Cryogenic Eng., AIP Conf.*, U. Balachandran Ed., vol. 58, 2012, pp. 125–132.
- [28] K. Han *et al.*, "Selected Ni alloy considerations for superconducting magnets," *IEEE Trans. Appl. Supercond.*, vol. 23, no. 3, Jun. 2013, Art. no. 7800204.
- [29] K. Han, Y. Xin, R. Niu, Y. Xin, and V. Toplosky, "Characterization of Nitronic-40 stainless steel shells," *IEEE Trans. Appl. Supercond.*, vol. 31, no. 5, 2021, Art. no. 7800105.
- [30] R. P. Walsh, K. Radcliff, J. Lu, and K. Han, "The low temperature mechanical properties of a Nitronic 40 forging," in *Proc. IOP Conf. Ser.: Mater. Sci. Eng.*, 2020, Art. no. 12001.
- [31] S. Araujo, N. Delpouve, L. Delbreilh, D. Papkov, Y. Dzenis, and E. Dargent, "Dielectric and calorimetric signatures of chain orientation in strong and tough ultrafine electrospun polyacrylonitrile," *Polymer*, vol. 178, Sep. 2019, Art. no. 121638.
- [32] F. Awaja, S. N. Zhang, and D. R. McKenzie, "Autohesion of semi-crystalline PEEK near and under the glass transition temperature," *Appl. Surf. Sci.*, vol. 282, pp. 571–577, Oct. 2013.
- [33] B. W. Chieng, N. A. Ibrahim, W. Yunus, and M. Z. Hussein, "Plasticized poly(lactic acid) with low molecular weight poly(ethylene glycol): Mechanical, thermal, and morphology properties," *J. Appl. Polym. Sci.*, vol. 130, no. 6, pp. 4576–4580, Dec. 2013.
- [34] L. A. Fillot, P. Hajji, C. Gauthier, and K. Masenelli-Varlot, "Thermomechanical history microstructure and impact effects on rigid PVC properties," *J. Appl. Polym. Sci.*, vol. 104, no. 3, pp. 2009–2017, May 2007.
- [35] H. Hagihara, K. Ito, and S. Kirnata, "Comprehensive study of altered amorphous structure in functionalized polypropylenes exhibiting high tensile strength," *Macromolecules*, vol. 46, no. 11, pp. 4432–4437, Jun. 2013.
- [36] Y. F. Lin *et al.*, "Structural evolution of hard-elastic isotactic polypropylene film during uniaxial tensile deformation: The effect of temperature," *Macromolecules*, vol. 51, no. 7, pp. 2690–2705, Apr. 2018.
- [37] N. Tortorella and C. L. Beatty, "Morphology and mechanical properties of impact modified polypropylene blends," *Polym. Eng. Sci.*, vol. 48, no. 11, pp. 2098–2110, Nov. 2008.
- [38] X. D. Wang *et al.*, "Non-covalently functionalized graphene strengthened poly(vinyl alcohol)," *Mater. Des.*, vol. 139, pp. 372–379, Feb. 2018.
- [39] B. H. Yuan, C. L. Bao, L. Song, N. Hong, K. M. Liew, and Y. Hu, "Preparation of functionalized graphene oxide/polypropylene nanocomposite with significantly improved thermal stability and studies on the crystallization behavior and mechanical properties," *Chem. Eng. J.*, vol. 237, pp. 411–420, Feb. 2014.
- [40] S. Zhou *et al.*, "The porous structure and mechanical properties of injection molded HA/PA66 scaffolds," *Int. Polym. Process.*, vol. 29, no. 4, pp. 454–460, Aug. 2014.
- [41] M. B. Kasen, G. R. MacDonald, D. H. Beekman, and R. E. Schramm, "Mechanical, electrical, and thermal characterization of G-10CR and G-11CR glass-cloth/epoxy laminates between room temperature and 4 K," *Adv. Cryog. Eng. (Mater)*, vol. 26, pp. 235–244, 1980.
- [42] R. M. Niu *et al.*, "Aging effect of Zylon," *IEEE Trans. Appl. Supercond.*, vol. 28, no. 3, Apr. 2018, Art. no. 7800104.